JOURNAL OF SOLID STATE CHEMISTRY 102, 213–225 (1993)

Structural Transitions in $LiNbO_3$ and $NaNbO_3$

APURVA MEHTA AND ALEXANDRA NAVROTSKY

Princeton Materials Institute and Department of Geological and Geophysical Sciences, Princeton University, Princeton, New Jersey 08544

AND NOBAHIRO KUMADA AND NOBUKAZU KINOMURA

Institute of Inorganic Synthesis, Yamanishi University, Kofu, Japan

Received August 12, 1991; in revised form May 21, 1992; accepted May 26, 1992

The ilmenite form of $NaNbO_3$ was synthesized hydrothermally. The ilmenite form of $LiNbO_3$ was synthesized by ion exchanging the ilmenite form of $NaNbO_3$. These transform irreversibly to the stable orthohombic form of $NaNbO_3$ and the lithium niobate form of $LiNbO_3$ at temperatures higher than 900 K. The energetics of the transformation was studied through differential scanning calorimetry and transposed temperature drop calorimetry. The calorimetric results show that the ilmenite form of $NaNbO_3$ is metastable by 5.5 (±1.3) kJ/mole and the ilmenite form of $LiNbO_3$ is metastable by 9.8 (±4.1) kJ/mole. Differential scanning calorimetry suggests that the $LiNbO_3$ transformation occurs in two steps. The enthalpy difference between the ilmenite and the lithium niobate structures for $LiNbO_3$ is compared with the difference in the lattice energies of the two structures predicted by H. J. Donnerberg, S. M. Tomlinson, C. R. A. Catlow, and O. F. Schirmer (*Phys. Rev. B* **40**, 11909, 1989) on the basis of an ionic model and is in good agreement with the calculations. This small energy difference lends credence to the $LiNbO_3$ defect model proposed by D. M. Smyth ("ISAF '86—Proceedings of the Sixth IEEE International Symposium on Applications of Ferroelectrics," p. 115, June 1986). The determination of the metastability of the ilmenite form of $NaNbO_3$ puts a limit on the tolerance factor for the stability of the perovskite structure.

Introduction

In an ABO_3 compound, if the A and the B cations are of approximately the same size and small enough to occupy oxygen octahedra, the compound adopts a sesquioxide structure with either a random or an ordered arrangement of cations. The sesquioxide structure is formed by an approximately hexagonal close-packed arrangement of oxygens. The cations (M) occupy two-thirds of the octahedral holes. These MO_6 units share vertices, edges, and/or faces. Let the two occupiable octahedral sites (out of three along the hexagonal c axis) be labeled A and B. If both sites, A and B, are occupied by identical atoms or occupied on average equally by the same set of atoms, the structure is disordered, with Al_2O_3, Cr_2O_3, and Fe_2O_3 as common examples. If the octahedral sites are arranged in a periodic sequence, an ordered sesquioxide structure forms. There are two common ordered arrangements of the A and the B sites: AB–BA, for which the structure is called the ilmenite type, after the mineral $FeTiO_3$; and AB–AB, for which the structure is called the lithium niobate type, with $LiNbO_3$ as the most com-

0022-4596/93 $5.00

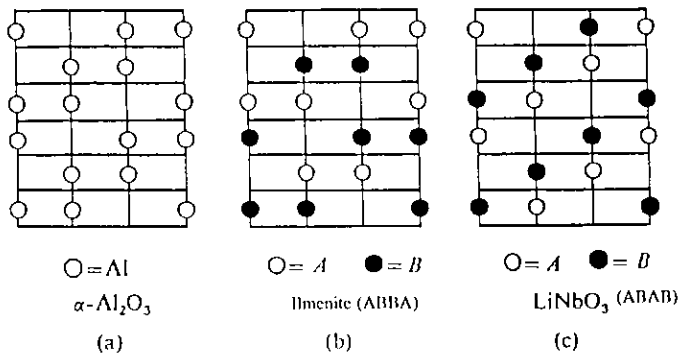

FIG. 1. Representation of the sesquioxide structure showing the disordered (a, corundum) and the two-ordered (b, ilmenite, and c, lithium niobate) subfamilies of structures. The horizontal lines represent the close-packed oxygen planes. The cations occupy the octahedral holes.

mon example. Figure 1 shows portions of the two ordered sesquioxide structures.

The commercial importance of $LiNbO_3$ is based on its electrooptic and nonlinear optical properties. These properties are intimately connected with the occurrence of ferroelectricity in $LiNbO_3$. Ferroelectricity can be supported in the noncentrosymmetric lithium niobate type ($R3c$) sesquioxide structure. However, the centrosymmetric ilmenite-like ($R\bar{3}$) structure could not possibly exhibit ferroelectricity. Crystallization of $LiNbO_3$ in a slightly different ordered version of the sesquioxide structure would then dramatically alter its technologically important properties. It is, therefore, of technological interest to study the stability of the various sesquioxide forms of $LiNbO_3$.

There is further interest in the structural stability of various sesquioxide forms from the point of view of defect chemistry of $LiNbO_3$. The common form of $LiNbO_3$ is crystallized from a congruent melting composition. This composition is highly Li deficient; it has Li/(Li + Nb) = 0.486 (*1–3*). The Li deficiency is accommodated by cation vacancies and cation antisite defects (*4, 5*). $LiNbO_3$ can be made oxygen deficient on reduction. It has been proposed that in congruent $LiNbO_3$ the oxygen lattice is kept intact and the nonstoichiometry is accommodated by changing the cation defect concentrations (*6*). Based on precise X-ray diffraction data (*7*), the point defects in congruent $LiNbO_3$ have been modeled as vacancies on Nb sites and Nb on Li sites. Smyth (*5*) proposed that these complex cation defects in lithium niobate structure can be understood by viewing them as simple Li vacancies in the local ilmenite-type cation stacking sequence. Figure 2 demonstrates Smyth's proposal schematically. The pro-

$LiNbO_3$	V_{Li}^{1} ($LiNbO_3$)	$V_{Nb}^{5}Nb_{Li}^{4}$ ($LiNbO_3$)	V_{Li}^{1} (ilmenite)	Ilmenite
V	*V*	*V*	*V*	*V*
Li	Li	Li	Li	Li
Nb	Nb	Nb	Nb	Nb
V	*V*	*V*	*V*	*V*
Li	$\{V_{Li}\}$	$\{Nb_{Li}^{\cdots\cdot}\}$	Nb	Nb
Nb	Nb	$\{V_{Nb}^{\prime\prime\prime\prime\prime}\}$	$\{V_{Li}\}$	Li
V	*V*	*V*	*V*	*V*
Li	Li	Li	Li	Li
Nb	Nb	Nb	Nb	Nb

FIG. 2. Cation stacking sequences along the hexagonal *c* axis of the sesquioxide structure illustrating the defect model proposed by Smyth (*2*). The experimental evidence suggests the defects in $LiNbO_3$ to be the ones represented in the middle column. Smyth's model views them as defects in the ilmenite stacking sequence (second column from the right).

proposal implies that the energetic difference between the two structure types, the ilmenite and the lithium niobate, is small in comparison with defect energies. The ease of accommodation of a Li defect in the ilmenite structure would then more than compensate for the metastability of the ilmenite-like stacking of Li and Nb. Parameterized ionic model calculations of Donnerberg *et al.* (*8*) support this argument and place the metastability of the ilmenite form of $LiNbO_3$ at 0.1 eV (9.6 kJ/mole).

In 1985, Kumada *et al.* (*9*) succeeded in crystallizing and quenching $LiNbO_3$ in the ilmenite structure, indicating that the energetic difference between the two ordered sesquioxide structures is indeed surmountable. This brief paper is still the only reported synthesis of $LiNbO_3$ in the ilmenite structural form. It did not report detailed chemical analysis or measure any physical properties but is nevertheless a significant contribution to crystal chemistry as it opens the gates to such measurements. Here we present the first reported study of the detailed chemical and thermochemical analysis of the solid solution of the ilmenite form of the $NaNbO_3$–$LiNbO_3$ system.

The stable structural form for $NaNbO_3$ is perovskite. It is believed that the difference between the ionic radii of Na and Nb is too large to easily form a sesquioxide (e.g., ilmenite) structural form of $NaNbO_3$. Thermochemical determination of the metastability of the ilmenite form of $NaNbO_3$ would address the fundamental crystal chemical question of the tolerance of the sesquioxide structure to accommodate two cations with very different sizes.

Experimental Methods

Synthesis of the Ilmenite-Type Materials

The ilmenite form of $NaNbO_3$ was prepared hydrothermally from hydrated sodium polyniobate and sodium hydroxide. The ilmenite form of $NaNbO_3$ was then ion exchanged, to replace Na with Li, to form the ilmenite structural form of $LiNbO_3$. Experimental details are described elsewhere (*9, 10*). This paper discusses the analysis of four different samples (pure $NaNbO_3$ + three different batches of Li-exchanged samples), referred to as S1–S4. The ion-exchange conditions for the four batches of samples are listed here:

S1 0-hr exchange: pure $NaNbO_3$
S2 12-hr exchange at 573 K in a $LiNO_3$ solution
S3 15-hr exchange at 573 K in a $LiNO_3$ solution
S4 25-hr exchange at 573 K in a $LiNO_3$ solution

The results of chemical analysis and the detailed X-ray diffraction analysis (see below) indicate that not all the Na was replaced by Li even after 25 hr of ion exchange.

Chemical Analysis

A fraction (~50 mg) of sample was dissolved in hydrofluoric acid and the solution was analyzed for Na and Nb using an inductively coupled argon plasma (ICP) spectrometer (Perkin–Elmer ICP-6000). The ICP peaks were converted to the elemental concentrations by comparing them against the peaks of elemental standards dissolved in hydrofluoric acid and diluted to approximately match the concentrations found in the sample. The ratio of Na to Nb was used to estimate the amount of $NaNbO_3$ remaining in each batch of the Li-exchanged sample. ICP analysis for Na was performed on high-purity congruent $LiNbO_3$ (sample supplied by R. J. Holmes, Bell Laboratories, AT&T) to check for the background Na contamination picked up under normal handling and laboratory exposure.

One of the Li-exchanged samples (S2) was also microchemically analyzed in a JEOL JXA-8600 electron microprobe.

Nb_2O_5 and the ilmenite form of $NaNbO_3$ were used as Nb and Na standards. The sample and the standards were mounted in epoxy, and the surface was polished to a 0.25-μm finish and then coated with a thin layer of carbon. The analysis was performed using a 10.33-nÅ probe in a 5-μm raster mode. It was feared that Na would migrate under the beam giving rise to an erroneous microanalysis. To characterize the Na drift, a 10.33-nÅ probe was stationed on a grain of $NaNbO_3$ and the decay of the signal was studied as a function of time. The sodium signal decayed less than 10% in over a minute, the maximum time of the analysis. Several different Li-exchanged $NaNbO_3$ grains were analyzed to obtain a statistically significant Na content. The microstructure of the sample was studied using a secondary electron detector and a backscatter detector.

X-ray Diffractometry

X-Ray measurements were performed on a Scintag PAD V automated diffractometer using Cu$K\alpha$ radiation. For determining the lattice parameters, measurements were done at a scan rate of 1° 2θ per minute and a chopper increment of 0.03° 2θ. Before determining the peak positions, the background of the diffraction pattern was subtracted and the peaks due to the $K\alpha_2$ radiation were removed. The lattice parameters were refined using a least-squares procedure.

Calorimetry

Two types of calorimetric experiments were performed: differential scanning and transposed temperature drop. A Setaram DSC 111 TG with a silver block was used in a horizontal configuration for scanning calorimetry on one of the Li-exchanged samples (S2). Calorimetry was performed from 298 to 1073 K at a heating rate of 5 K/min. The crucible for the DSC analysis was of platinum. The procedure for the DSC measurements was to scan the empty crucible, from 298 to 1073 K, three times and average the runs to obtain the "blank" reading. The crucible was then filled with fine-grain alumina of 99.9% purity, which was fired at 1773 K and dried at 403 K. Three heating scans were performed on alumina. After the "blank" scan was subtracted, the DSC power output was compared to the heat capacity of alumina (*11*) to obtain a calibration curve. The platinum crucible was then cleaned, dried, and filled with the sample. The sample was subjected to two consecutive heating cycles. Between the two cycles the sample was kept at 1073 K for an hour. From the DSC power outputs the "blanks" were subtracted and the results were converted to heat capacity values by using the alumina calibration curve. All the measurements were performed in air. Due to the limited amount of available sample and a large amount (~100 mg) of sample required for a DSC run, DSC measurements were performed on only one batch of the Li-exchanged samples (S2).

For the transposed temperature drop calorimetry, high temperature Tian–Calvet-type calorimeters operating at 977 and 1057 K were used [described in detail elsewhere (*12, 13*)]. The experiments consisted of dropping a platinum capsule containing the sample from 295 K into the hot calorimeter. The sample was retrieved, cooled to room temperature (295 K), weighed, and dropped again. The heat effect associated with each drop experiment was measured. The heat effect associated with the first drop consisted of three contributions: the heat content of platinum, the heat content of the sample, and the enthalpy of the irreversible transformation (e.g., the transformation from the ilmenite structural type to the lithium niobate structural type). The heat effect associated with the second drop consisted of only two contributions: the heat content of platinum and that of the transformed sam-

TABLE I

ICP ANALYSIS FOR THE Li EXCHANGED $NaNbO_3$ SAMPLES

	Sample	Na/Nb (wt%)	$NaNbO_3$ (mole%)
Congruent $LiNbO_3$	—	$3.53 \pm 0.36 \times 10^{-2}$	Background 0.14
Li-exchanged $NaNbO_3$	S2	3.61 ± 0.47	14.58
	S3	2.00 ± 0.14	8.07
	S4	$8.93 \pm 0.27 \times 10^{-1}$	3.61

ple. Therefore, the difference between the heat effects for the two drops measured the enthalpy of transformation from the metastable structure to the stable structure (refer to Table IV).

Results and Discussion

Chemical Analysis:

Table I shows the results of the ICP Na and Nb analysis. The amount of Na detected in congruent $LiNbO_3$ is two orders of magnitude lower than the levels detected in the ion-exchanged material. Therefore, essentially all of the Na in the ion-exchanged material is a remnant from the process of ion exchange, and not from any other laboratory source of sodium contamination. Using this assumption, the atomic ratios of Na to Nb are converted to ratios of $NaNbO_3$ to $LiNbO_3$.

Figure 3 shows backscatter electron images of one of the Li-exchanged $NaNbO_3$ samples (S2). It has a very unusual grain size distribution. Roughly half of the sample is composed of particles of 5–15 μm, whereas the other half of the sample is made up of submicrometer particles that tend to cluster in 50- to 100-μm clumps. Furthermore, most of the larger grains show striations along one of the crystallographic directions. Careful examination of these striations with the secondary electron probe suggests that the striations are cracks rather than evidence of compositional variation. No compositional variation in any of the grains was visible in the backscatter images. The clumps of the submicrometer particles appear darker than the other larger particles because the probe diameter is much larger than some of the smaller particles of the clumps and hence the probe excites a large fraction of the surrounding, lower-molecular-weight epoxy, resulting in seemingly lower average molecular weight for the clump of submicron grains.

Table II lists the results of the Na and the Nb microanalysis performed on one of the Li-exchanged $NaNbO_3$ samples (S2). The analysis was performed on seven larger (5- to 15-μm) grains and two submicrometer particles. The mole percentage $NaNbO_3$ in a grain shows a grain-to-grain variation (from 9 to 20%). The grain-to-grain variation of the $NaNbO_3$ content is much larger than the statistical uncertainty of the measurement ($\pm$0.46 mole% $NaNbO_3$). The analysis of the two submicrometer particles is found to be within the range of the variation found in the larger grains albeit the overall $NaNbO_3$ content is on the lower side of the range. This observation could be an artifact due to the impossibility of excluding all the surrounding epoxy matrix from the sampling volume of the electron probe. The average $NaNbO_3$ content of the sample found by averaging the analyses of the seven larger grains (13.49 mole%) is very similar to the amount determined by the ICP analysis (14.58 mole%). As no variation in the atomic mass number contrast was detected within grains (and no separate $NaNbO_3$ grains were found), it is concluded that, at least on the micrometer scale, the sample is a solid solution $(Li_{0.86}Na_{0.14})NbO_3$.

X-Ray Diffraction

Na, Li, and Nb have very different X-ray scattering factors from Fe and Ti (the cations in the standard ilmenite, $FeTiO_3$). Therefore, the peak intensities of the pow-

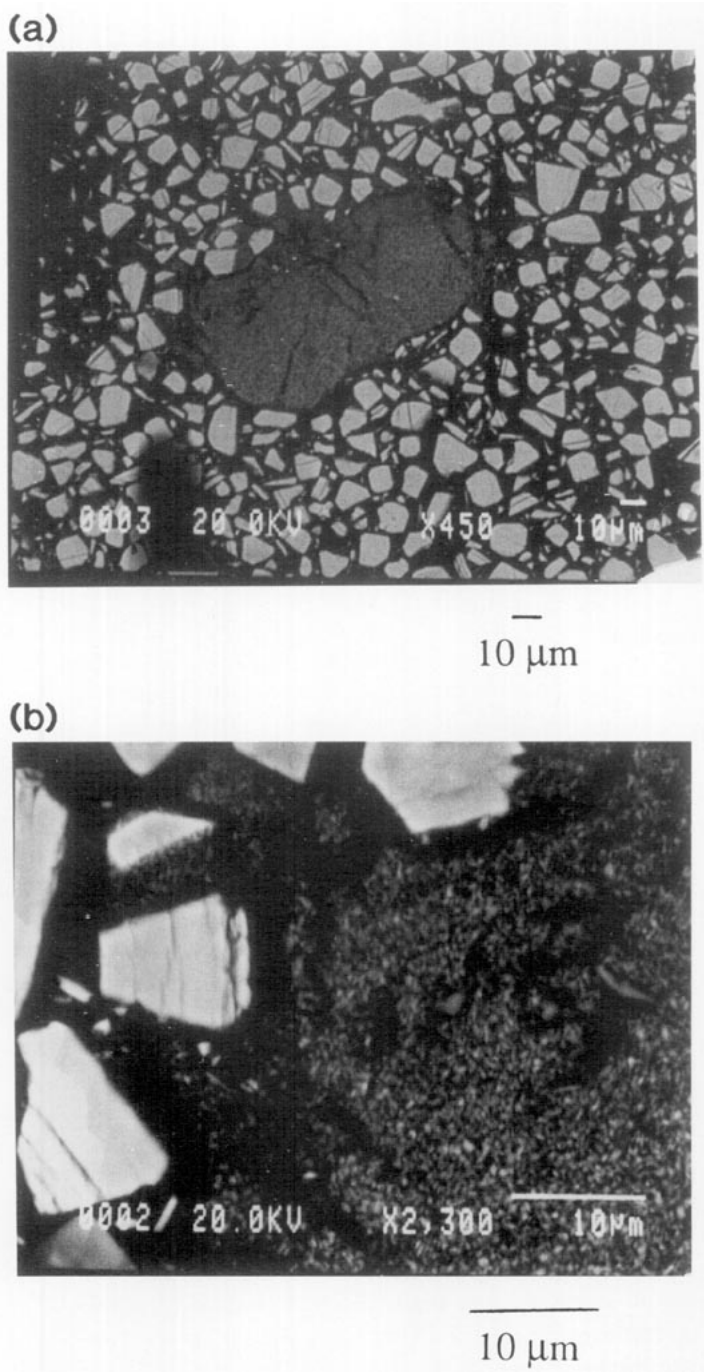

FIG. 3. Backscattered electron images of Li-exchanged $NaNbO_3$ (see text for interpretation).

der diffraction patterns of the Li-exchanged $NaNbO_3$ look very different from the diffraction pattern of $FeTiO_3$ (for example, the most intense peak of Li-exchanged material is not visible in $FeTiO_3$). Therefore, for a positive structural identification of the Li-exchanged $NaNbO_3$ as the ilmenite form of $(Li,Na)NbO_3$, the powder diffraction pattern of the ilmenite-type $LiNbO_3$ was simulated using the atomic positions of Fe and Ti (*14*) as fractional coordinates for Li and Nb. The peak positions and intensities of the powder diffraction pattern of the Li-exchanged material closely resembled the simulation. The lattice parameters (for a hexagonal cell) of the ilmenite form were refined using a least-squares procedure utilizing the actual peak positions. Table III list the lattice parameters, the unit-cell volume, and the mole percentage Na for the four batches of the sample. The lattice parameters for the ilmenite form of samples are in good agreement with previously reported measurements (*9, 10*) for samples for which no detailed chemical analysis was reported. The lattice parameters of the ilmenite phase are plotted against their analyzed sodium content in Fig. 4. The ion-exchanges samples do show small variations in a and c (and molar volume) with Na/(Na + Li) which, to a first approximation, fall on straight lines with the corresponding parameters for $NaNbO_3$ ilmenite. This is a further indication that the Na in the ion-exchanged samples is in substitutional solid solution. From the relationship of the lattice parameters to the Na content of the sample, one can con-

TABLE II

MICROPROBE ANALYSIS OF ONE OF THE LI-EXCHANGED $NaNbO_3$ (S2)

Grain No.	$NaNbO_3$ (mole%)	2 SD
1	10.80	0.46%
2	9.65	0.46%
3	20.42	0.46%
4	15.20	0.46%
5	13.81	0.46%
6	14.68	0.46%
7	9.90	0.46%
Average	13.49	
Submicrometer particles		
1	12.84	0.15%
2	11.27	0.18%

TABLE III

LATTICE PARAMETERS OF THE ILMENITE SAMPLES

Sample	%$NaNbO_3$	Cell parameters in S.G. $R\bar{3}$ a (Å)	c (Å)	Cell volume (Å^3)
S1	100.00	5.334 (1)	15.63 (1)	385.3
S2	14.58	5.225 (1)	14.38 (1)	340.0
S3	8.07	5.215 (1)	14.37 (2)	338.4
S4	3.61	5.213 (1)	14.33 (2)	337.3

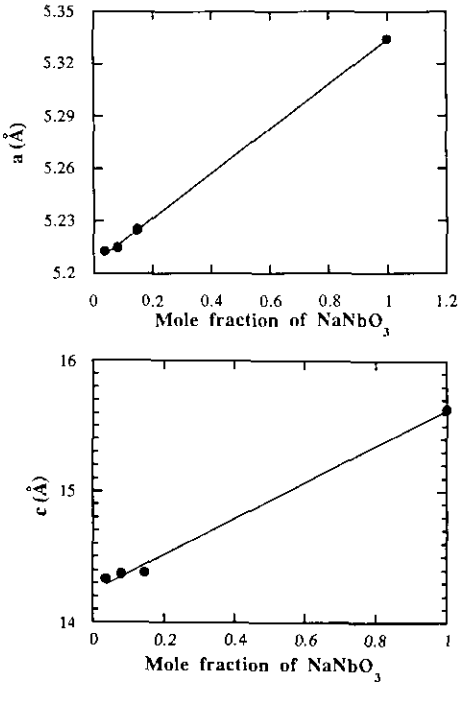

FIG. 4. Lattice parameters of the ilmenite phase versus the mole fraction of $NaNbO_3$.

TABLE IV

THERMODYNAMIC CYCLE FOR THE TRANSFORMATION OF ILMENITE FORM OF $(Li_{1-x}Na_x)NbO_3$

$Li_{1-x}Na_xNbO_3$ (ilmenite, 295 K) → $(1 - x)$ $LiNbO_3$ (ilmenite, 295 K) + $x NaNbO_3$ (ilmenite, 295 K)

$LiNbO_3$ (ilmenite, 295 K) + $NaNbO_3$ (ilmenite, 295 K) → $LiNbO_3$ (lithium niobate, 295 K) + $NaNbO_3$ (ortho., 295 K)

$LiNbO_3$ (lithium niobate, 295 K) + $NaNbO_3$ (ortho., 295 K) → $LiNbO_3$ (lithium niobate, TK) + $NaNbO_3$ (ortho., TK)[a]

$LiNbO_3$ (lithium niobate, TK) + $NaNbO_3$ (ortho., TK) → $LiNbO_3$ (lithium niobate, 295 K) + $NaNbO_3$ (ortho., 295 K)

$Li_{1-x}Na_xNbO_3$ (ilmenite, 295 K) $\xrightarrow{\Delta H_{1st\ drop} - \Delta H_{2nd\ drop}}$ $(1 - x)LiNbO_3$ (lithium niobate, 295 K) + $xNaNbO_3$ (ortho., 295 K)

[a] T is the calorimeter temperature: 1057 or 977 K.

clude that the first (and the only) reported synthesis of $LiNbO_3$ ilmenite by Kumada *et al.* (9) had about 4 mole% $NaNbO_3$ in it.

The X-ray diffraction patterns of the material recovered after the DSC runs and the transposed temperature drops identified them as two-phase mixtures of the lithium niobate form of $LiNbO_3$ and the orthorhombic form of $NaNbO_3$ by comparison with the reported diffraction pattern for those materials (JCPDS Card Files 20-631 and 33-1270). The actual peak positions were refined to give the lattice parameters for lithium niobate phase as space group $R3c$ (161), $a = 5.14(1)$ Å, $c = 13.89(5)$ Å, and the orthorhombic phase as space group $Pbma$ (57), $a = 5.56(1)$ Å, $b = 15.52(5)$ Å, $c = 5.50(1)$. The results of the X-ray analysis indicate unmixing of Li-exchanged $NaNbO_3$ on transformation into a two-phase mixture of a lithium niobate form of $LiNbO_3$ and a perovskite form of $NaNbO_3$, with these being essentially pure end members.

Calorimetry

Table IV shows a thermodynamic cycle for the transformation of the ilmenite-type $LiNbO_3$–$NaNbO_3$ solid solution (to the lithium niobate form of $LiNbO_3$ and the orthorhombic form of $NaNbO_3$) in a transposed temperature drop measurement. The enthalpy of transformation for

$$Li_{(1-x)}Na_xNbO_3 \text{ (ilmenite)} \rightarrow (1 - x)LiNbO_3 \text{ (lithium niobate)} + xNaNbO_3 \text{ (ortho.)} \quad (1)$$

at 295 K is calculated from the difference between the heat associated with the first and the second transposed temperature drops. Table V summarizes the calorimetric results for the four ilmenite samples. Each sample lost a small fraction of its weight on the first drop, and no further loss was observed on the second drop. The origin of this mass loss (and hence the volatiles) is unknown and no thermochemical correction was made. The observed enthalpy of reaction (1) appears to vary quite strongly from sample to sample. We call this observed enthalpy the enthalpy of decomposition. Note that the enthalpy of decomposition contains contributions, in principle, from the unmixing of the solid solution and the transformation of the unmixed end members. This will be discussed further below.

Differential scanning calorimetry (DSC) was performed on one of the of Li-exchanged $NaNbO_3$ samples (S2) to obtain an additional independent confirmation of the enthalpy of transformation [enthalpy of reaction (1)], DSC was also used to study the transformation pathway. Figure 5 shows two DSC curves. The first sample run (upper curve) began with one of the Li-exchanged $NaNbO_3$ samples (S2), which was com-

TABLE V

ENTHALPIES OBSERVED IN TRANSPOSED TEMPERATURE DROP CALORIMETRY ON THE ILMENITE FORM OF $(Li_{1-x}Na_x)NbO_3$

Sample/ caloric temp	Drop no.	Number of measurements	Average % mass loss	ΔH (J/g)	Uncertainty[a] (J/g)	ΔH_{Decomp}[b] (kJ/mole)
S1	1	4	0.35	593.59	5.90	
1057 K	2	4	0.00	572.88	4.76	−5.46 ± 1.24
S2	1	4	0.60	516.68	9.08	
1057K	2	4	0.00	628.09	12.32	−16.75 ± 2.26
S3	1	4	0.36	447.65	7.56	
977 K	2	4	0.00	547.61	2.98	−14.92 ± 1.21
S4	1	4	1.46	465.59	6.53	
977 K	2	4	0.00	542.35	5.46	−11.46 ± 1.27

[a] Uncertainty is reported as two standard deviations of the mean.

[b] $\Delta H_{Decomp} = \Delta H_{1st\ drop\ avg} - \Delta H_{2nd\ drop\ avg}$.

pletely transformed to the stable form of the material (see X-ray Diffraction under Results). The second sample run began with the transformed material. There were no further observable phase transformations involved in the second sample run (lower curve). The enthalpy for each run was obtained by integrating the heat capacity with respect to temperature to give the enthalpy for each run. The enthalpy associated with the first DSC sample run, ${}^1\Delta H_{obs}$, can be written as

$$ {}^1\Delta H_{obs} = \int_{295\ K}^{T} Cp_{ut}\, dT + \Delta H_T + \int_{T}^{1073\ K} Cp_t\, dT \quad (2) $$

where Cp_{ut} is the vibrational heat capacity of the ilmenite form of sample, Cp_t is the

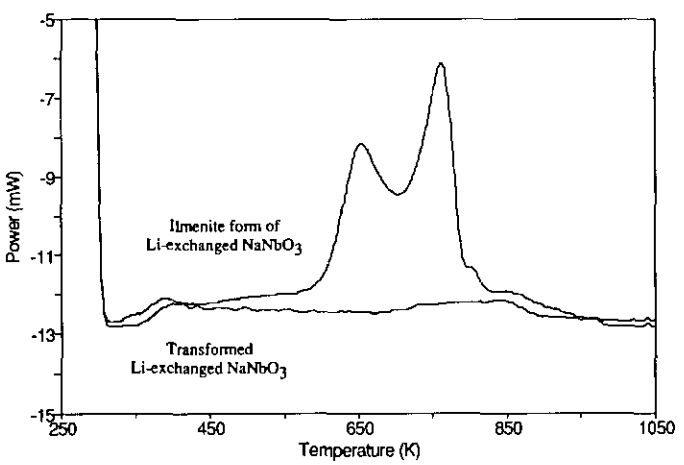

FIG. 5. DSC runs on the Li-exchanged $NaNbO_3$. The top plot is the run for the starting material and the bottom plot is the run for the sample that has already transformed. A positive deviation from the baseline (second sample run) indicates an exothermic transformation reaction.

vibrational heat capacity of the transformed form of the sample (which is mostly the lithium niobate form of $LiNbO_3$), T is the temperature of transformation, and ΔH_T is the enthalpy of transformation at the temperature of transformation. The heat effect associated with the second DSC sample run, ${}^2\Delta H_{obs}$, can be written as

$$ {}^2\Delta H_{obs} = \int_{295\ K}^{1073\ K} Cp_t\, dT. \qquad (3) $$

If the vibrational heat capacities of the two ordered sesquioxide forms, the ilmenite (Cp_t) and the lithium niobate (Cp_{ut}), are assumed to be similar, then the difference between Eqs. (2) and (3) gives the overall enthalpy of decomposition at the temperature of transformation. The enthalpy of decomposition of the ilmenite form of Li-exchanged $NaNbO_3$ (S2) obtained via scanning calorimetry (-14.9 ± 2.0 kJ/mole) is in good agreement with the value obtained via transposed temperature drop calorimetry (-16.8 ± 2.3 kJ/mole). The error in scanning calorimetry is estimated from the reproducibility of the three alumina standard runs.

Another interesting result of the scanning calorimetry is the double-peaked nature of the first sample run. The first and the smaller of the two peaks corresponds to about 40% of the heat effect and the second and the larger peak corresponds to the other 60% of the heat effect. Approximately 14 mole% (15.5 wt%) of the sample is $NaNbO_3$ and the enthalpy of transformation of the ilmenite form of $NaNbO_3$ (S1) is found to be -5.5 kJ/mole (whereas the observed heat effect is 15 kJ/mole). Therefore the peak due to the $NaNbO_3$ transformation would correspond to only 5% of the heat effect. Therefore, neither of the two peaks can correspond to the $NaNbO_3$ transformation. The double-peaked form of the DSC run, however, can be interpreted as further evidence of the existence of two very disparate grain size distributions in the sample. The ilmenite form of $LiNbO_3$ is thermodynamically unstable. It is quenchable in the unstable form due to kinetic hindrance to nucleation of the transformation process. It is therefore reasonable to assume that the kinetics of transformation is determined by the rate of nucleation. If nucleation is heterogeneous and begins at the free surface then the rate of nucleation (and hence the rate of transformation) would be proportional to the temperature and the specific surface area of the material. The smaller (submicrometer—Fig. 3) particles would have larger specific surface area and thus would have a large propensity to nucleate the transformation at a given temperature. In other words the smaller grains would transform at a lower temperature in the DSC. The ratio of the area under the two DSC peaks would then be approximately proportional to the fraction of the sample in the two different grain size groups. The DSC results indicate that approximately 40% of the sample is composed of submicrometer grains, an estimate that agrees well with the visual observations of the sample in the electron microprobe. The DSC measurements were not repeated on other samples due to a limited amount of available material.

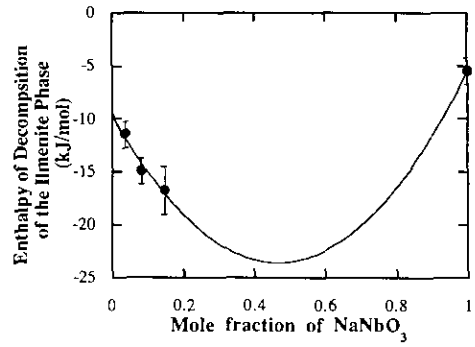

FIG. 6. The 295 K enthalpy of transformation of the ilmenite form of $Li_{1-x}Na_xNbO_3$ as a function of Na content (X) (reaction 1).

Figure 6 shows the observed enthalpy of

decomposition of the ilmenite form of material across the $NaNbO_3$–$LiNbO_3$ solid solution. The solid curve is the best quadratic regression fit to the data and is represented by the equation

$$\partial H = -5.457x - 9.839(1 - x) - 63.24x(1 - x) \quad (4)$$

where x is the mole fraction of $NaNbO_3$ in the sample, the coefficient of the first term (-5.5 ± 4.1 kJ/mole) is the enthalpy of the perovskite form (with respect to the ilmenite form) of the $NaNbO_3$ end member, the coefficient of the second term (-9.8 ± 4.1 kJ/mole) is the enthalpy of the lithium niobate form (with respect to the ilmenite form) of the $LiNbO_3$ end member, and the coefficient of the third term of the equation (-63 ± 18 kJ/mole) is the regular solution parameter for unmixing of the two end members in the ilmenite solid solution. The uncertainties were estimated by imposing a 90% confidence interval on the data set. A large negative (exothermic) enthalpy of unmixing suggests that the solid solution of the two ilmenite endmembers (i.e., the Li-exchanged $NaNbO_3$ samples) could be extremely unstable with respect to unmixing. However, the metastable ilmenite solid solution was produced by ion-exchange under conditions where the nucleation of the separate phases was probably hindered. Unmixing might proceed once temperature is raised. The unmixed end-member compositions would then transform to their stable polymorphs (lithium niobate for $LiNbO_3$ and perovskite for $NaNbO_3$). Although, there is enough of a difference in the ionic radii of Na and Li to expect some positive heat of mixing, the extremely large magnitude of the regular solution parameter, 63 kJ/mole, is somewhat surprising.

The above analysis suggests that for the reaction $LiNbO_3$ (ilmenite) → $LiNbO_3$ (lithium niobate), the enthalpy is -9.8 ± 4.1 kJ/mole. Donnerberg *et al.* (*8*) estimated the transformation enthalpy from the ilmenite to the lithium niobate form of $LiNbO_3$ to be -0.1 eV (-9.6 kJ/mole). The excellent agreement between the experimentally determined value and the estimate from lattice energy calculations validates the ionic modeling methods employed by Donnerberg *et al.* The estimate of the metastability of the ilmenite form of $LiNbO_3$ also strongly supports Smyth's (*5*) defect model for $LiNbO_3$. A small transformation energy of 10 kJ/mole with respect to defect formation energies of a few hundred kJ/mole is consistent with a defect accommodation mechanism in which the defects are incorporated in altered cation stacking sequences to effect an overall energetic savings [refer to (*8*) for details].

Among the various sesquoxide structures, ilmenite seems to be the most common room temperature and pressure structure. At higher pressure and temperature quite frequently the lithium niobate structure is stabilized [as in the case of $MnTiO_3$ and $FeTiO_3$ (*15*, *16*)]; however, $LiNbO_3$ and $LiTaO_3$ are the only known examples of lithium niobate structures stable at low temperature. It is intriguing to note that the only crystallographic difference between the lithium niobate and the ilmenite structure is that in the lithium niobate structure, the *A*–*B* (e.g., Li–Nb) dipoles are aligned along a crystallographic direction (along the hexagonal *c* axis of the crystal), whereas in the ilmenite structure, these dipoles are stacked opposing each other giving the lattice a center of symmetry (see Fig. 1). The highly polarizable nature of the *A*–*B* dipoles in $LiNbO_3$ and $LiTaO_3$ and the dipole alignment makes these materials ferroelectric (the ferroelectricity cannot be exhibited in the centrosymmetric ilmenite crystal symmetry.). Is it then plausible that there is a correspondence between the high polarizability of the *A*–*B* dipoles in $LiNbO_3$ and $LiTaO_3$ and the energetic stability of the lithium niobate structure for these materials? $LiTaO_3$ has a lower Curie temperature than

$LiNbO_3$ and hence it is less polarizable than $LiNbO_3$. It could be argued that if there is a one-to-one correspondence between the lattice polarizability and the energetic stability of the lithium niobate structure over the ilmenite structure, then the ilmenite phase of $LiTaO_3$ would indeed be energetically less stable than the lithium niobate phase; however, it would not be as unstable as the ilmenite phase of $LiNbO_3$ is with respect to the lithium niobate phase. Synthesis and the measurement of the enthalpy of the ilmenite $LiTaO_3$ would test the above hypothesis.

The ilmenite phase of $NaNbO_3$ was found to be metastable with respect to the perovskite phase by 5.5 ± 1.2 kJ/mole (see Table V). The very small energetic metastability (6 kJ/mole) of $NaNbO_3$ in the sesquioxide (ilmenite) form over the perovskite form of the material gives insight into the tolerance of the sesquioxide structure for cations of disparate sizes. One can look at this through the distortion and the stability of the perovskite structure which competes with the ilmenite structure.

It is thought that the compound ABO_3 crystallizes in the perovskite structure if the A ions are large enough to form a close-packed array with the oxygens and the B ions are small enough to occupy the oxygen octahedra. The ideal perovskite structure has the cubic space group symmetry of $Pm3m$. Deviations from the ideal geometric requirements for the cubic structure distort the lattice. A useful way of measuring the geometrical distortion of the perovskite structure was developed by Goldschmidt (*17*) in the form of the tolerance factor, defined as

$$t = (r_A + r_O)/1.414(r_B + r_O) \qquad (5)$$

where r_A, r_B, and r_O are the ionic radii of A, B, and O ions, respectively. As the two cations become smaller and more comparable in size the tolerance factor decreases and the structure distorts to a lower than cubic symmetry. If the cations are much smaller than the oxide ions then even distorted perovskite structures become unstable. The most probable structure for the compound then is one of the hexagonal sesquioxide structures.

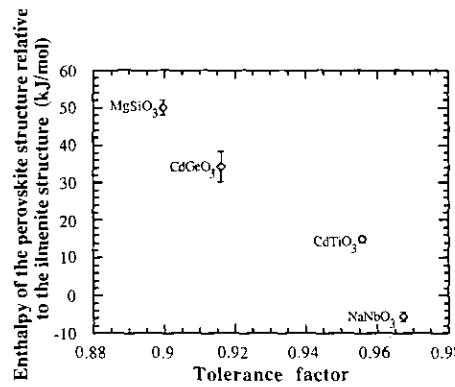

FIG. 7. Enthalpy of the perovskite structure with respect to the ilmenite structure as a function of tolerance factor.

A few of the ABO_3 compounds have been crystallized in both perovskite- and ilmenite-like structures. The enthalpy of the perovskite-like structure with respect to the ilmenite structure has been measured for four of these compounds: $NaNbO_3$ [this study], $CdTiO_3$ (*18, 19*) $CdGeO_3$ (*18*), and $MgSiO_3$ (*18, 20*). Figure 7 shows enthalpy of the perovskite structure with respect to the ilmenite structure (negative values means that the perovskite is energetically more stable) as a function of the tolerance factor. The tolerance factors were calculated based on Shannon and Prewitt ionic radii (*21, 22*). The large central cation in the two highly distorted perovskites, $CdGeO_3$ and $MgSiO_3$, was assumed to be 8-coordinated [see Takayama-Muromachi and Navrotsky (*23*). A monotonic and almost linear relationship is seen between the tolerance factor and the enthalpy of transformation. The relationship suggests that in the vicinity of tolerance factor of 0.96 the ilmenite structure is approximately (energetically) as sta-

ble as a perovskite structure. The empirical relationship suggests that for a tolerance factor lower than 0.96, an ABO_3 compound would preferentially crystallize in the ilmenite-like structure rather than the perovskite-like structure, at least at low temperature where the $T\,\Delta S$ term is not important. The perovskite structure is normally denser and quite frequently has higher entropy than the ilmenite structure (*24*). Hence quite frequently for a low-temperature stable ilmenite compound, the perovskite structure is stabilized at high pressure and temperature by its denser molar volume and higher entropy.

Acknowledgments

The assistance of R. Haushalter of Exxon Research and Engineering Company in simulating the X-ray diffraction pattern and that of M. Borcsik in performing ICP are greatly appreciated. This study was supported by the National Science Foundation (Grant DMR 89-12549).

References

1. J. R. Carruthers, G. E. Peterson, M. Grasso, and P. M. Brindenbaugh, *J. Appl. Phys.* **42,** 1846 (1971).
2. R. L. Holman, "Proceedings of the 14th University Conference in Ceramic Science, November 7–9, 1977, Raleigh, NC" (H. Palmour, R. F. Davies, and T. M. Hare, Eds.), Plenum, New York (1979).
3. R. J. Holmes and D. M. Smyth, *J. Appl. Phys.* **55,** 3531 (1984).
4. R. J. Holmes and W. J. Minford, *Ferroelectrics* **75,** 63 (1987).
5. D. M. Smyth, "ISAF '86—Proceedings of the Sixth IEEE International Symposium on Applications of Ferroelectrics," p. 115 (June 1986).
6. P. Lerner, C. Legras, and J. P. Dumas, *J. Cryst. Growth* **3,** 231 (1968).
7. S. C. Abrahams and P. Marsh, *Acta Crystallogr. B* **42,** 61 (1986).
8. H. J. Donnerberg, S. M. Tomlinson, C. R. A. Catlow, and O. F. Schirmer. *Phys. Rev: B* **40**(17) 11909 (1989).
9. N. Kumada, N. Ozawa, F. Muto, and N. Kinomura, *J. Solid State Chem.* **57,** 267 (1985).
10. N. Kinomura, N. Kumata, and F. Muto, *Mater. Res. Bull.* **19,** 299 (1984).
11. D. A. Ditmars and T. B. Douglas: *J. Res. Natl. Bur. Stand.* **75A**(5), 401 (1971).
12. A. Navrotsky, *Phys. Chem. Minerals* **2,** 89 (1977).
13. N. L. Ross, M. Akaogi, A. Navrotsky, J. Susaki, and P. McMillan, *J. Geophys. Res.* **91,** 4685 (1986).
14. B. A. Wechsler and C. T. Prewitt, *Am. Mineral.* **69,** 176 (1984).
15. J. Ko, N. E. Brown, A. Navrotsky, C. T. Prewitt, and T. Gasparik, *Phys. Chem. Minerals* **16,** 727 (1989).
16. K. Leinenweber, W. Utsumi, Y. Tsuchida, and T. Yagi, *Phys. Chem. Minerals,* in press.
17. V. M. Goldschmidt, *Skr. Nor. Vidensk-Akad. Oslo* **1,** 1 (1926).
18. A. Navrotsky, *Prog. Solid State Chem.* **17,** 53 (1987).
19. J. M. Neil, A. Navrotsky, and O. J. Kleppa, *Inorg. Chem.* **10,** 2076 (1971).
20. T. Ashida, S. Kume, E. Ito, and A. Navrotsky, *Phys. Chem. Minerals* (1988).
21. R. D. Shannon and C. T. Prewitt, *Acta Crystallogr. A* **32,** 751 (1976).
22. R. D. Shannon and C. T. Prewitt, *Acta Crystallogr. B* **25,** 925 (1976).
23. E. Takayama-Muromachi and A. Navrotsky, *J. Solid State Chem.* **72,** 244 (1988).
24. A. Navrotsky, "Perovskite—A Structure of Great Interest to Geophysics and Materials Science" (A. Navrotsky and D. J. Weidner, Eds.), p. 67, Am. Geophys. Union, Washington, DC, (1989).